Rheological investigation of magnetic sensitive biopolymer composites: effect of the ligand grafting of magnetic nanoparticles

Alberto Varela Feijoo, Modesto T Lopez-Lopez, Cécilia Galindo-Gonzalez, Stéphanie Stange, Thi Thuy Nguyen, Fayna Mammeri, Souad Ammar-Merah, Alain Ponton

Rheologica Acta (2020) 59:165–176
https://doi.org/10.1007/s00397-020-01191-y

ORIGINAL CONTRIBUTION

Rheological investigation of magnetic sensitive biopolymer composites: effect of the ligand grafting of magnetic nanoparticles

Alberto Varela Feijoo[1] · Modesto T. Lopez-Lopez[2,3] · Cécilia Galindo-Gonzalez[1] · Stéphanie Stange[1] · Thi Thuy Nguyen[4,5] · Fayna Mammeri[4] · Souad Ammar-Merah[4] · Alain Ponton[1]

Received: 20 August 2019 / Revised: 31 December 2019 / Accepted: 22 January 2020 / Published online: 18 February 2020

Abstract

This study investigated the steady shear flow and viscoelastic properties of composite materials elaborated by introduction of positively charged polyol-made maghemite nanoparticles (NPs) in aqueous solutions of negatively charged sodium alginate polymers. Two different ligands were covalently attached to the particle surface, the 3-aminopropyl triethyloxysilane (APTES) and the 3,4-dihydroxyphenylethylamine (DOPA), and their effect on the general rheological and magneto-rheological behaviors of the resulting composites was highlighted. Indeed, the experiments revealed that the increase of low shear viscosity and the viscoelastic moduli in the linear viscoelastic domain can be correlated to the nature of the two ligands inducing either compact or loose aggregates between positively charged NPs and negatively charged biopolymer chains. These field-induced microstructures have been qualitatively observed by optical microscopy under applied magnetic field.

Keywords Nanoparticles · Sodium alginate · Composites · Magnetic field · Magnetorheology

Introduction

Nanocomposites derived from organic matrix and inorganic nanoparticles (NPs) have attracted increasing attention because of their unique properties emerging from the synergistical combination of the attractive functionalities of both components (Jeon and Baek 2010). On the one hand, NPs have a much higher surface-to-volume ratio, compared to conventional micron-sized particles. As a result, interparticle forces such as van der Waals and electrostatic forces become stronger. On the other hand, polymers offer a wide range of individual properties that can be explored in nanocomposite materials: mechanic, thermic, optic, and hydrophilic (Ridi et al. 2014). These nanocomposites offer new technology and business opportunities for all sectors of industry (Camargo et al. 2009). The choice of natural polymers, obtained from renewable sources, allows additionally obtaining environmental friendly materials with interesting properties such as biocompatibility, stability in aqueous media, and biodegradability. In a first stage, stimuli-responsive nanocomposite hydrogels containing natural polymers have been studied for their response to changes in pH and temperature (Haraguchi et al. 2012). Although, magnetic stimulation shows advantages over other types of stimuli in term of penetration and invasiveness, particularly for biological tissues.

Thereby, smart composites materials obtained by incorporating magnetic NPs in biopolymer matrices opened new perspectives in terms of functionalities and

Electronic supplementary material The online version of this article (https://doi.org/10.1007/s00397-020-01191-y) contains supplementary material, which is available to authorized users.

✉ Alain Ponton
alain.ponton@univ-paris-diderot.fr

[1] Laboratory Matière et Systèmes Complexes, Université de Paris, UMR-CNRS 7057, Condorcet building CC 7056, 75205 Paris Cedex 13, France

[2] Department of Applied Physics, University of Granada, Granada, Spain

[3] Instituto de Investigación Biosanitaria IBS.Granada, Granada, Spain

[4] Laboratory ITODYS, Université de Paris, UMR-CNRS 7086, Lavoisier building CC 7090, 75205 Paris Cedex 13, France

[5] Department of Advanced Materials Science and Nanotechnology, University of Science and Technology of Hanoi, Vietnam Academy of Science and Technology, 18 Hoang Quoc Viet, Hanoi, Vietnam

applications. The possibility to control material properties by an external magnetic field provides to this magnetically responsive biopolymer-based composites (Liu and Urban 2010) (Schexnailder and Schmidt 2009) new and promising functionalities for drug delivery (Brazel 2009), sensoring (Richter et al. 2008), and tissue engineering (Van Vlierberghe et al. 2011). A key point in the design of these materials is the surface modification of their constituting magnetic NPs. Their successful integration within the hydrogel polymeric matrices is mainly dependent on their chemical functionalization and on the nature of their surface ligands. The formation of strong and stable bonds, between these NPs and the polymer chains, avoids their phase separation under an applied magnetic field. Typically, in water, alginates, thanks to their anionic carboxylate groups, are polyelectrolytes. These polyelectrolytes may strongly interact electrostatically with magnetic NPs bringing on their surface positively charged ligands, like amino groups (Laurent et al. 2008).

In the literature, several alginate-based magnetic nanocomposites are described. Their preparation and their evaluation for biomedical applications are often reported, but their magneto-rheological behavior is seldom detailed. For instance, composites made from alginate/poly(vinylalcohol) (Alg/PVA) coupled to iron oxide NPs were already prepared and their zero magnetic field viscoelastic properties were measured using a rheometric dynamic mechanical analyzer (Nishio et al. 2004). Composites made from iron oxide NPs in situ synthetized into alginate beads were also described, and their magnetic properties were studied for drug delivery applications (Morales et al. 2008); but once again, their magneto-rheological behavior was not explored. In this context, we prepared, in a previous work (Galindo-Gonzalez et al. 2014), magnetic iron oxide (maghemite) NPs, using the polyol process and we functionalized them by bifunctional ligands able to be covalently attached to the particle surface in one hand and to electrostatically interact with the alginate chains in the other hand. We also investigated their magneto-rheological properties, and we evidenced net differences in their mechanical responses in presence of an external magnetic field. We did not try at that time to modulate the interactions between the NPs and the polymer chains. Also, we did not investigate the link between the change in the rheological properties under an applied magnetic field and the microstructure of the considered composites. In the present study, we propose to address the question of the nature of the bounded ligands on the NPs surface on the whole magneto-rheological properties of magnetic alginate-based nanocomposites, with a special emphasis on their local microstructure thanks to an advanced optical visualization of their chain arrangements.

Materials and methods

Sample preparation

Nanoparticles

Maghemite (γ-Fe_2O_3) NPs were synthesized by forced hydrolysis of iron acetate salts in diethylene glycol (Basti et al. 2010) followed by a repeated boiling water washing (Hanini et al. 2011). The obtained nanoparticles with a diameter of 11 ± 2 nm (Fig. 1) were then subsequently functionalized by 3-aminopropyl triethyloxysilane (APTES) and 3,4-dihydroxyphenylethylamine (DOPA), using surface sol-gel chemistry (Galindo-Gonzalez et al. 2014) and surface cation complexation reaction (Fouineau et al. 2013), respectively (Fig. 2).

As previously evidenced, APTES and DOPA grafting does not affect the structure of the particles. It improves their separation, balancing their mutual magnetic attraction in water by their electrostatic repulsion thanks to their positively charged ammonium surface groups. The positive surface charge of the produced nanohybrids was confirmed by Zeta potential measurements performed on their aqueous suspension using the Nanosizer Malvern instrument operating with a laser of 633 nm, for different pH values (Fig. 3). As expected, the recorded curves indicate a shift of the isoelectric point (IEP) according the nature of the coating. It is, of course, close to the pKa of water (IEP ~ 7) for nude particles and close to pKa of a free amino molecule (IEP ~ 9) for particles grafted with APTES. Surprisingly, it is smaller than this value for particles coated with DOPA, while both APTES and DOPA leave the same terminal amino group.

To understand this feature, we have to keep in mind the fact that DOPA, with its catechol group, is a much more rigid molecule compared to the aliphatic type APTES one. As a consequence, a denser coating with DOPA is expected. Indeed, it was already established that for a dense

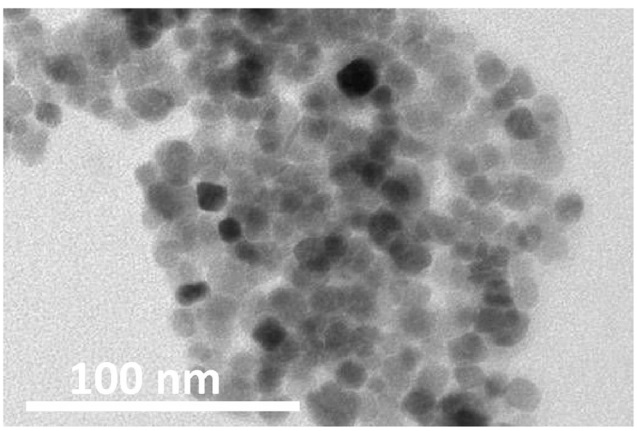

Fig. 1 Transmission electron microscopy (TEM) image of an assembly of polyol-made maghemite NPs

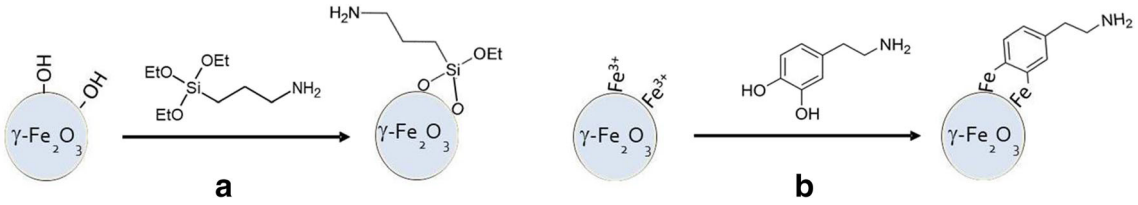

Fig. 2 Schematic representation of the functionalization of maghemite NPs by **a** APTES and **b** DOPA

mercaptoundecanoic coating on a gold NP surface, the carboxylic/carboxylate pKa displays a positive shift of at least 2 units compared to its value for free-standing molecules (Wang et al. 2011; Charron et al. 2012). Such a feature was also reported on terminal carboxyl bearing thiols assembled on planar gold substrates (Creager and Clarke 1994; Kane and Mulvaney 1998), pointing out the effect of confinement on a surface. As the distance between the charges decreases, the electrostatic repulsion between carboxylates increases. Hence, denser coating smaller NPs have a larger shift in pKa. This explanation could be extended to the influence of the length of ligand carbon chain; ligands bearing shorter chains should develop a more intense electrostatic repulsion with each other and then exhibit a higher pKa shift. To the best of our knowledge, such a study was never performed on amino ligands. By extrapolation, one may assume that DOPA should exhibit a shift of its amino/ammonium pKa value compared to APTES, when attached to a same particle surface. As the distance between the positive charges decreases, the electrostatic repulsion between ammonium groups increases, leading to a shift to lower pKa values. The correlation between the pKa changes and the measurement of the IEP values leads to conclude that DOPA coating is denser than APTES one. Zeta experiments were repeated to confirm such tendency, and systematically, the measured "NPs-DOPA" IEP was found smaller, by at last two units, than the "NP APTES" one, the former being closer to 7, and the later being closer to 10.

Nanocomposites

The white dried powder of sodium alginate extracted from marine brown algae was dissolved, as-purchased, in deionized water (50 g L^{-1}), to obtain an anionic polyelectrolyte in which the carboxylate anion charges are counterbalanced by those of sodium cations. The dissolution was carried out at room temperature (RT) under mechanical stirring (300 rpm) for 14 h. In the same time, solid APTES- and DOPA-grafted NPs were dispersed in deionized water by mixing a few minutes with a vortex, and then by ultrasonication at RT. Afterwards, deionized water was added to a known volume of the stock solution of sodium alginate. After a mechanical stirring of 5 min, a volume of aqueous suspension of magnetic NPs was finally introduced to obtain the two studied samples with a constant sodium alginate concentration ($C_{alg} = 18$ g L^{-1}) while incorporating 1 vol.-% fraction ($\Phi_{NP\text{-}APTES}$ and $\Phi_{NP\text{-}DOPA}$) of APTES- and DOPA-grafted NPs, respectively. In practice, in-air thermogravimetry (TG) measurements were performed to determine the weight ratio of the coating species for all the prepared hybrids, NPs-DOPA and NPs APTES. So, the mass of hybrid powder, m, was then systematically corrected from this contribution, m_{corr}, and the corresponding volume is obtained by dividing this corrected mass by the maghemite volumic mass, ρ. So, the particle volume fraction is then equal to the ratio between this calculated volume and the total volume of the prepared colloid. Fixing this volume fraction to 1% and the total solution volume to 2 mL allowed us to determine the corresponding m_{corr} and consequently the mass m of hybrids to be weighted.

Characterization

Magnetic measurements

The magnetic properties of maghemite NPs and their related APTES and DOPA hybrids were inferred from field-dependent magnetization curves measured on a Quantum Design MPMS-5S SQUID magnetometer at 300 K. The external magnetic field was varied in the − 4000 and + 4000 kA m^{-1} range. The studied powders were slightly compacted in a diamagnetic plastic sampling tube to avoid their displacement during measurements.

Table 1 Values of the parameters η_0, $\dot{\gamma}_C$, and n, corresponding to the best fits of experimental viscosity in the absence of applied magnetic field to a cross equation

	η_0 (Pa.s)	$\dot{\gamma}_C$ (s^{-1})	n (dimensionless)
Solution of 18 g/L of sodium alginate	1.10 ± 0.09	117 ± 9	0.26 ± 0.02
Solution of 18 g/L of sodium alginate and 1 vol.% of Fe_2O_3 particles coated with APTES	0.77 ± 0.06	121 ± 10	0.31 ± 0.03
Mixture of 18 g/L of sodium alginate and 1 vol.% of Fe_2O_3 particles coated with DOPA	1.92 ± 0.15	85 ± 7	0.28 ± 0.02

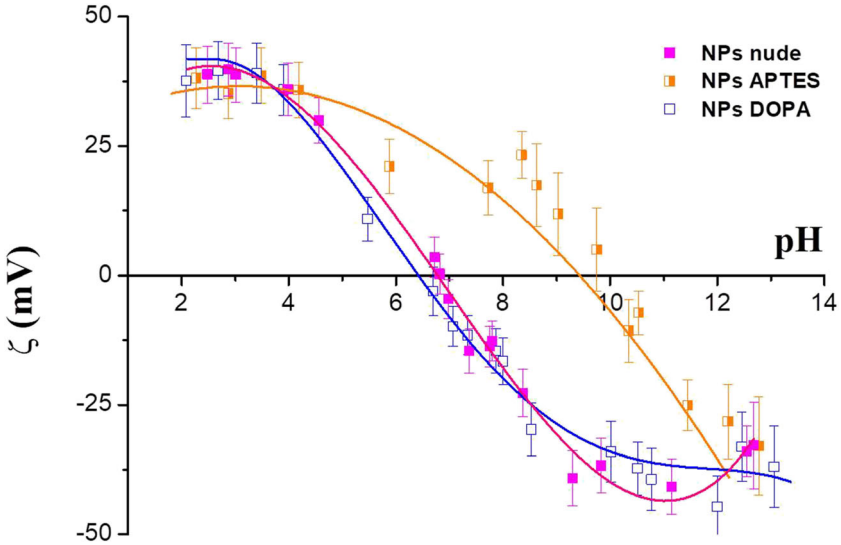

Fig. 3 Zeta potential variation as a function of the pH of as-produced maghemite NPs and their related APTES and DOPA hybrids dispersed in deionized water at the same concentration

Magneto-rheological measurements

The rheological measurements were performed at constant temperature (25.0 ± 0.1 °C) using a rheometer Mars II (Thermo Fisher Scientific, USA) fitted with a home-made magnetic cell allowing the application of a continuous and homogenous magnetic field to the sample during the measurements. This device was composed of a mechanical part and a magnetic part. The former was a cone and plate geometry (60 mm in diameter and an angle of 1°) made of non-magnetic material. The latter consisted of two coils which were mounted on both sides of the cone-plate geometry with the bottom plate placed in the upper part of the lower coil. This configuration allowed creating a homogeneous magnetic field perpendicular to the shear (e.g., parallel to the axis of rotation of the cone). A complete description and calibration of the device can be found in Galindo-Gonzalez et al. (2016)). Steady-state flow curves were obtained by increasing the shear rate from 0.01 to 2000 s^{-1}. The duration of each step was varied from 60 to 600 s depending on the value of imposed shear rate in order to measure stationary value of shear stress. For oscillatory measurements, a ramp of sinusoidal strain with constant frequency f = 1 Hz and variable amplitude between 10^{-4} and 10^{+3} was first applied. Frequency dependence of the elastic G′ and loss G″ moduli was then measured between 0.01 and 10 Hz at constant strain amplitude in the linear viscoelastic domain. When a magnetic field was applied, the following procedure was used: after insertion of the sample on the plate of magnetic cell, the magnetic field was switched on during 500 s. This waiting time was long enough to ensure an equilibrium state of the built up of field-induced structures in biopolymer network and thermal steady state.

Optical microscopic observations

Optical microscopy observation was carried out using a home-made setup special device (Galindo-Gonzalez et al. 2014) allowing the application of a magnetic field during the observations. Two moving permanent magnets were placed in slots of a non-magnetic circular plate. The positions of the two magnets were fixed by screws creating a magnetic field from 3.2 to 23.9 kA m^{-1} in the same range as for rheological measurements. A rectangular capillary filled with the prepared alginate-based nanocomposite solutions was placed at the middle of the plate perpendicularly to the direction of the magnetic field. The capillary was closed on both ends by modeling clay to avoid evaporation. The observation was performed by a Nikon microscope with a resolution objective of × 10 at one magnetic field value. The magnetic field was applied for 5 min before recording images, and the images were analyzed by a freeware software.

Results and discussion

Magnetic properties of NPs and nanohybrids

The room temperature variation of the magnetization of bare NPs and their related APTES- and DOPA-nanohybrids, as a function of the applied magnetic field, evidences a superparamagnetic behavior. Neither remanence nor coercivity have been measured at this temperature. Using the variation of the magnetization as a function of magnetic field M(H) curves (M expressed here per gram of hybrid powder), it is possible to estimate the amount x (weight percent) of the organic shell in the hybrid particles:

$$M(\text{hybrid}) = x \times M(\text{organic coating}) + (1-x) \times M(Fe_2O_3) \quad (1)$$

where M(hybrid), M(organic coating), and $M(Fe_2O_3)$ are the saturation magnetization of DOPA or APTES-coated particles, that of the organic shell alone and the saturation magnetization of nude particles respectively. These three values are determined graphically ($M(\text{NPs nude}) = 69.91\ Am^2\ kg^{-1}$, $M(\text{NPs APTES}) = 68.29\ Am^2\ kg^{-1}$, $M(\text{NPs-DOPA}) = 66.45\ Am^2\ kg^{-1}$.

So, considering the magnetization of the organic shell as equal to zero due to their diamagnetic nature x is found to be equal to 2.3 and 4.9 wt.% for NPS APTES and NPs-DOPA, respectively, in good agreement with TG results, confirming again the formation of a denser organic layer around Fe_2O_3 magnetic cores in the later compared to the former hybrids (Fig. 4).

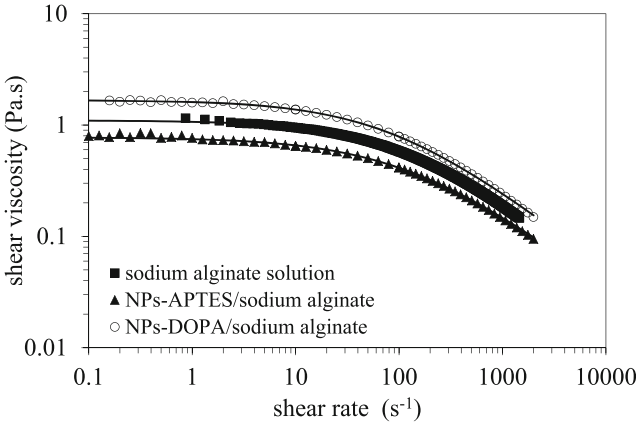

Fig. 5 Steady-state flow curves of the solution of 18 g/L of sodium alginate and the suspensions consisting of 18 g/L of sodium alginate and 1 vol.% of magnetic particles (either coated with APTES or DOPA, as indicated in the figure). The solid lines correspond to the best fits to a Cross equation—see Table 1 for values of the best fits

Rheological and magneto-rheological properties of the nanocomposites

Steady state

As shown in Fig. 5, steady-state flow curves of aqueous solution of sodium alginate without and with magnetic nanoparticles are characteristic of a shear-thinning behavior with an approximately constant value of the viscosity at low shear rate (η_0) followed by decrease of the viscosity when shear rate is increased above a critical shear rate. Cross equation (Eq. (2)) has been used successfully to fit this typical behavior for solutions of entangled polymers (Doublier and Launay 1981; Rayment et al. 1995; Wang et al. 1997; Ren et al. 2003).

$$\eta = \eta_\infty + \frac{\eta_0 - \eta_\infty}{1 + \left(\gamma/\dot{\gamma}_C\right)^{1-n}} \quad (2)$$

where η_0 and η_∞ are, respectively, limiting viscosities at zero and infinite shear rates. The parameter n is a rate constant characteristic of the flow behavior in the shear-thinning region. The infinite shear rate viscosity η_∞ was not obtained experimentally. It was fixed to $0.9\ 10^{-3}$ Pa s, the viscosity of the water at 25 °C.

The limiting viscosity at zero shear rate (η_0) is higher for the suspension containing nanoparticles coated with DOPA while it is smaller for the suspension containing nanoparticles coated with APTES. This intriguing and opposite behavior with respect to the magnitude of η_0 of suspensions with

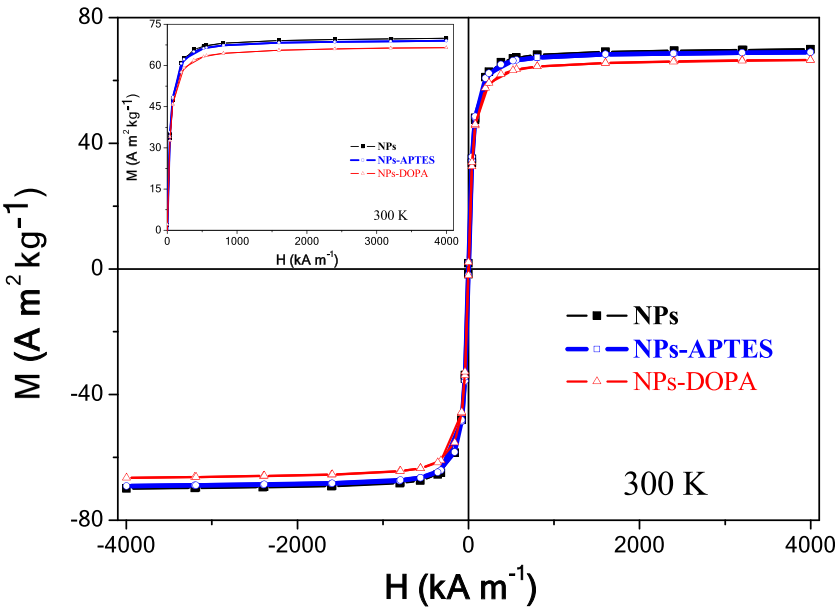

Fig. 4 Room temperature variation of the magnetization versus magnetic field of bare iron oxide NPs and their related nanohybrids. A zoom on the first quadrant of the loops is given in the inset

respect to the value of the alginate solution seem inconsistent with the prediction of Batchelor formula for the viscosity of a suspension of spherical particles (Batchelor 1977):

$$\eta_s = \left(1 + 2.5\varphi + 6.2\varphi^2\right)\eta_i \quad (3)$$

where η_s is the viscosity of the suspension of spherical particles, ϕ the volume fraction of particles (or particle aggregates), and η_i the viscosity of the carrier fluid. According to Eq. (3), since $\phi > 0$ the viscosity of the suspension should be higher than the viscosity of the carrier fluid. Then, the decrease of the viscosity at low shear rates come from the hypothetical trapping of polymer chains within particle aggregates of more or less spherical shape, so that η_i is considerably reduced with respect to the viscosity of the original sodium alginate solution, as a consequence of the reduction of the amount of free alginate polymer. Of course, trapping of alginate polymer within particle aggregates would increase the effective concentration of particle aggregates (i.e., ϕ), and the resulting η_s viscosity would be higher or smaller than the viscosity of the initial sodium alginate solution depending on the competition between these two opposite phenomena (decrease of the concentration of free polymer in the carrier fluid and increase of the effective concentration of particle aggregates).

Concerning the exponent n, it is characteristic for each polysaccharide and independent of the concentration inside the semi-dilute entangled regime. The typical values lie in the range $0.2 < n < 1$, and the physical meaning corresponds to the usual exponent in power law representations; a value of 1 will be representative of a Newtonian behavior and as the value becomes smaller, the shear-thinning behavior will be more significant. For our particular case, alginate solution of 18 g/L, the responsible of the shear-thinning behavior is the decrease of the entanglements and the reorganization of the chains when we increase the shear rate. The small increase of the value of n that we observe when we introduce both types of NPs indicate the presence of electrostatic interactions between NPs and polymer chains in the entangled network inducing the formation of more resistant entanglements and hindering the reorganization of the alginate chains by effect of the shear rate and, consequently, leading to a less significant shear-thinning behavior. Nevertheless, the magnitude of the effect on both systems is not the same with a higher increase in the exponent n for the case of APTES-coated than DOPA-coated NPs. This phenomenon is concerned by the different nature of both coatings, and thus, the different formed microstructure.

Let us now discuss on the origin of the particle aggregates. We should discard direct particle-particle interaction as the cause of aggregation. Maghemite particles of 10–12 nm in diameter are single domains from the magnetic point of view and, consequently, there is always magnetic interaction between them. However, particles used in this work are coated by ligands (APTES or DOPA) which would impart both steric and electrostatic repulsions. Steric and electrostatic repulsions act as a barrier that prevents from contact between the magnetic cores of the particles and, under this condition, Brownian motion dominates over magnetic attraction between particles, preventing from aggregation [(Rosensweig 1985)]. Our hypothesis is that the negatively charged alginate polymers interact electrostatically with the positive molecules coating the particles, giving rise to bridging flocculation between different particles. Note that this bridging flocculation should be the origin of aggregates on both systems (NPs-APTES and NPs-DOPA). However, there must be differences between both systems at the microscopic point of view. First, as evidenced in Fig. 3, the Zeta potential is more positive for NPs-APTES than for NPs-DOPA, i.e., there are more electrostatic interactions for the former than for the latter. In addition, there are differences with regard to the rigidity vs. flexibility of the particle-molecule bond, the former being considered as much more flexible than the later, as illustrated hereafter in Fig. 6.

We should then expect that in nanoparticle aggregates of NPs-APTES/sodium alginate system, each single alginate chain is attached to a nanoparticle (or aggregates of nanoparticles) at many different points and, thus, different particles are linked quite strongly, as depicted schematically in Fig. 7. The resulting particle aggregates in NPs-APTES/sodium alginate system should thus be robust, and quite magnetic, since the average distance between particles should be small and, consequently, the volume concentration of particles within these aggregates high.

On the contrary, DOPA-coated nanoparticles present a lower isoelectric point and, thus, the number of electrostatic links with alginate chains in each of these nanoparticles (or aggregates of nanoparticles) is smaller. As a consequence, we expect that aggregates in NPs-DOPA/sodium alginate system are loose and large flocculi, consisting of a considerably smaller concentration of magnetic particles and polymers than aggregates in NPs-APTES/sodium alginate system (Fig. 7).

Since the concentration of particles and polymer chains in both systems is the same, a higher concentration of both within the aggregates implies a smaller concentration of aggregates within the system—and on the contrary, a smaller concentration of both within the aggregates implies a higher concentration of aggregates within the suspensions. This hypothesis qualitatively justifies the stronger increase of the exponent n of Eq. (2) in the case of APTES-coated than DOPA-coated

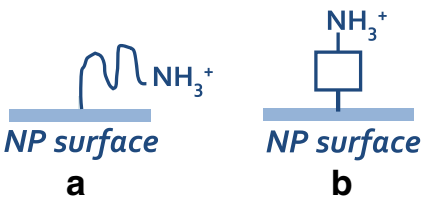

Fig. 6 Schematic representation of the amine-particle bond in the **a** APTES- and **b** DOPA-based hybrids

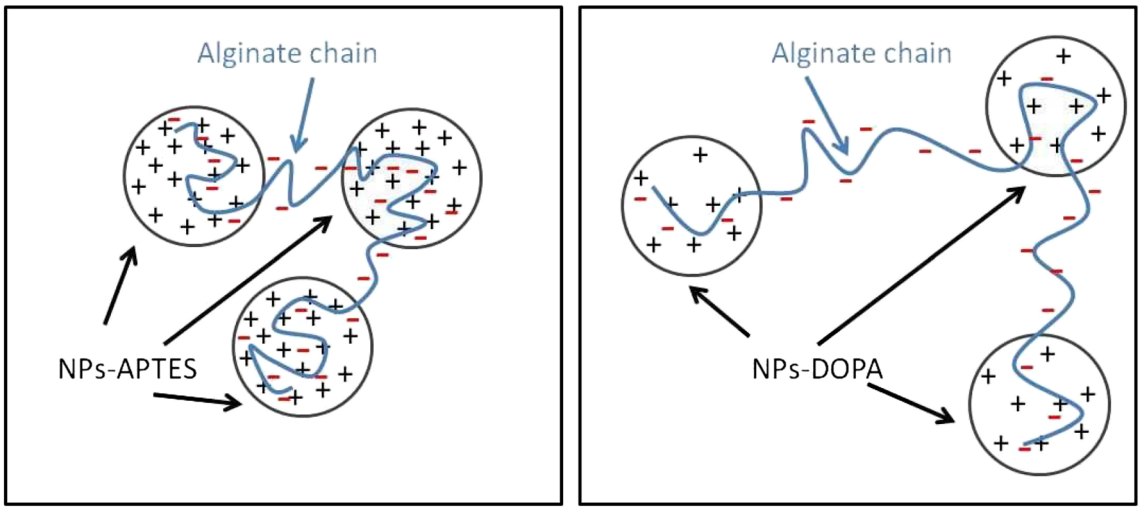

Fig. 7 Sketch of structure of particle/polymer aggregates in NPs-APTES/sodium alginate systems and in NPs-DOPA/sodium alginate systems. + represents positive charges on the particle surface and − negative charges in the polymer chain. Note that the number of links between polymer and particle is higher in NPs-APTES/sodium alginate system than in NPs-DOPA/sodium alginate system

NPs. We will see below that this hypothesis also explains the rheological results in the presence of applied magnetic field and, in addition, it is supported by microscopic observations.

Finally, the value of the critical shear rate ($\dot{\gamma}_C$) gives us an indication of the onset of shear rate for the beginning of the shear-thinning behavior. As in the case of η_0, we observe opposite behaviors with respect to the magnitude of $\dot{\gamma}_C$ of suspensions with respect to the value of the alginate solution. This contradictory effect comes precisely from the different values of η_0. As it has shown previously, the analysis of the onset of the shear-thinning behavior in terms of a limiting shear rate above we start to disentangle the polymer chains, it becomes confusing when we analyze the effect of the concentration.

Magnetoviscous effect

The steady-state flow curves as a function of shear rate for two values of the applied magnetic field is shown in Fig. 8. For the sake of discussion, the viscosity values in the absence of applied magnetic field are also shown.

As observed, at low shear rate values, both systems display a typical magnetoviscous effect, consisting of an enhancement of the viscosity as the magnetic field is increased. This enhancement of the viscosity with respect to the off-state diminishes as the shear rate increases, becoming negligible at values of the shear rate of the order of 10 s^{-1}, which is also typical of the magnetoviscous effect. This effect is characteristic of suspensions of magnetic particles, either ferrofluids or magnetorheological fluids, as a consequence of the formation of particle structures or drops of particle condensation, elongated in the direction of the applied magnetic field (Bossis et al. 2013). Ferrofluids are suspensions of single-domain magnetic particles of a size typically smaller than 20–30 nm (Rosensweig 1985), whereas magneto-rheological fluids are constituted by multidomain magnetic particles of a diameter of the order of 1 μm. Magnetoviscous effect (MVE) is usually quantified by the increment of the viscosity at a given field, η_H, with respect to zero field, η_0, normalized by the zero field viscosity:

$$MVE = \frac{\eta_H - \eta_0}{\eta_0} \tag{4}$$

As observed (Fig. 9), the MVE is considerably higher for NPs-APTES/sodium alginate system than for NPs-DOPA/sodium alginate system. Our hypothesis for this is as it follows. Magnetoviscous effect arises mainly as a consequence of the resistance of magnetic field-induced particle structures to flow—we neglect here the effect of rotational viscosity that could account only for a maximum MVE of 0.015 (Odenbach and Thurm 2002). Since we have considered above that in the absence of applied magnetic field there are some particle/

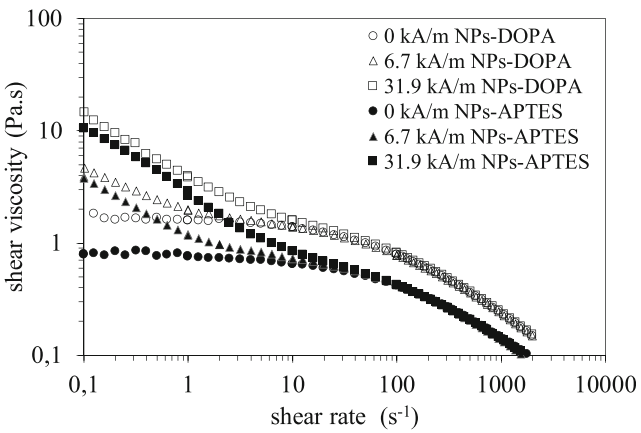

Fig. 8 Viscosity as a function of shear rate for NPs-DOPA/sodium alginate system and NPs-APTES/sodium alginate system for three different values of the applied magnetic field (kA m^{-1}): 0, 6.7, 31.9

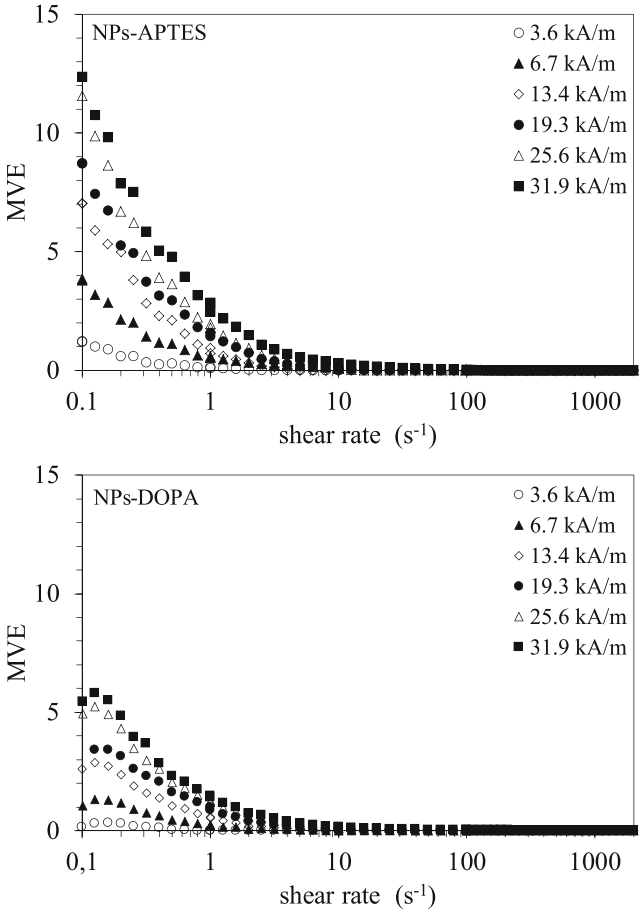

Fig. 9 Magnetoviscous effect (Eq. (4)) for **a** NPs-APTES/sodium alginate system and **b** NPs-DOPA/sodium alginate system for different values of the applied magnetic field (values indicated in the figure)

polymer aggregates (Fig. 7), structures induced by the magnetic field should consist of column-like arrangements constituted by a large number of those aggregates aligned along the field direction. Note that in response to the applied magnetic field, each of the aggregates would also deform, in order to minimize its free energy balanced by the bulk free energy due to the demagnetizing field, which would tend to stretch the aggregate in the direction of the applied field, and the energies associated to the surface tension and the role of the polymer that would tend to maintain a spherical shape for the aggregates (Lopez-Lopez et al. 2014).

The strength of the field-induced arrangements (and thus the intensity of the MVE) would be determined by the strength of the magnetostatic interaction between different particle/polymer aggregates and the resistance of individual elongated aggregates to be inclined by hydrodynamic forces. For a given amount of magnetic material within the system, the strength of both phenomena depends mainly on the concentration of magnetic material within the aggregates, which accordingly to previous discussion should be higher in NPs-APTES/sodium alginate system, which would justify the stronger MVE effect in this system.

Shear stress at 0.1 s^{-1}

If we consider the value of shear stress at a shear rate of 0.1 s^{-1} in the absence of magnetic field, we found experimentally a non-negligible value for NPs-DOPA/sodium alginate system (0.28 Pa), whereas it is much smaller (but also non-negligible) for NPs-APTES/sodium alginate system (0.08 Pa). From this result, we could justify that in the NPs-DOPA/sodium alginate system, there is some macroscopic ordering in the absence of field—we could even speak about particle aggregates so large that they percolate the measuring gap. This hypothesis is confirmed by microscopic observations (see "Microscopic observations"). On the contrary, there are only relatively smaller aggregates in NPs-APTES/sodium alginate system.

From the increments of the stress at 0.1 s^{-1} with respect to zero field, two behaviors are observed (Fig. 10) depending on the range of magnetic field. For magnetic field lower than about 10 kA m^{-1}, APTES presents slightly higher increments of stress supporting previous discussion of MVE. For magnetic field higher than about 10 kA m^{-1}, APTES presents lower increments of the stress. This result confirms that DOPA is highly flocculated and that this flocculation is reinforced in the presence of applied magnetic field.

Oscillatory regime

Amplitude sweeps. Viscoelastic linear region As shown in Fig. 11, the variation of elastic G′ and viscous G″ moduli as a function of strain amplitude and constant frequency (1 Hz) is typical of viscoelastic material with an initial pseudoplateau at low values of the strain amplitude, which is associated to the linear viscoelastic domain (LVD), followed by a decreasing trend at large values of the strain amplitude. As for any system showing magnetic field-dependent rheological properties, the values of both G′ and G″ increase with the magnetic field strength. Note, nevertheless, that at zero-field (data not shown

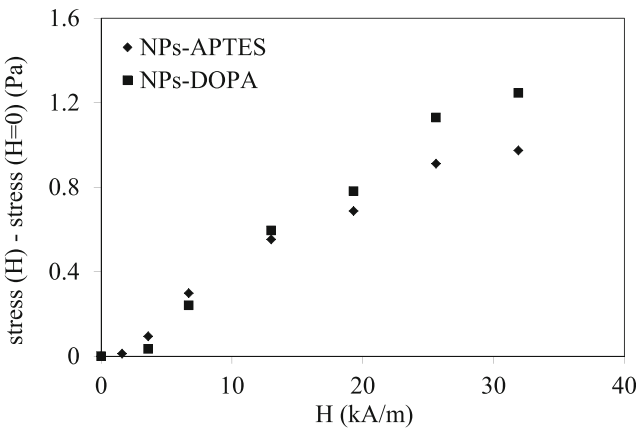

Fig. 10 Increment of shear stress at 0.1 s^{-1} with respect to zero field as a function of magnetic field for NPs-APTES/sodium alginate system and NPs-DOPA/sodium alginate system

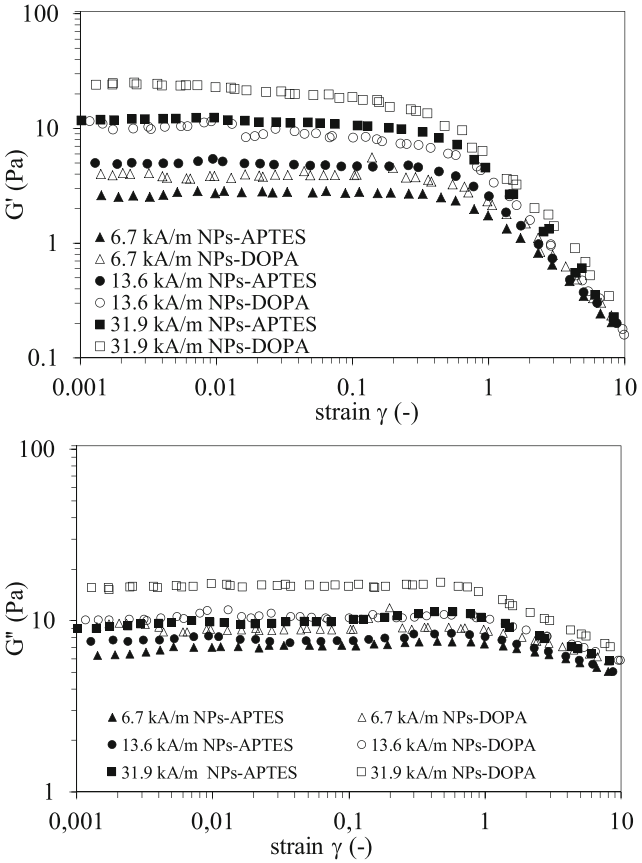

Fig. 11 Variation of elastic G′ and viscous G″ moduli as a function of strain amplitude (and constant frequency of 1 Hz) for NPs-APTES/sodium alginate system and NPs-DOPA/sodium alginate system at different values of applied magnetic field

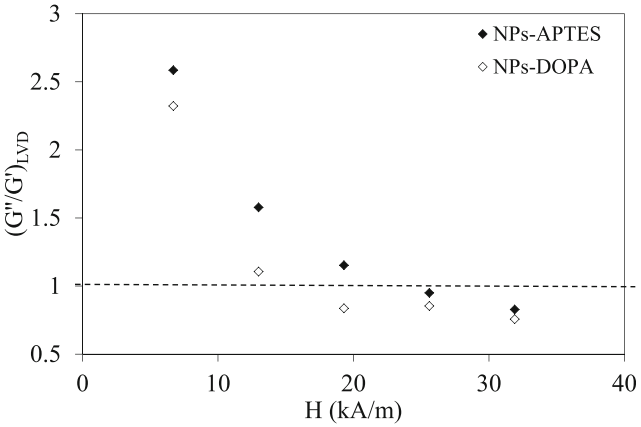

Fig. 12 Variation of the ratio of viscous modulus by elastic modulus G′ in the linear viscoelastic domain (LVD) as a function of magnetic field for NPs-APTES/sodium alginate system and NPs-DOPA/sodium alginate system

here for brevity), G′ is smaller than G″ by a factor of 6, although the increase of G′ with the field is faster, which gives rise G′ values larger than G″ at the largest magnetic field strengths. In other words, we could say that our systems are more liquid than solid at low value of the applied magnetic field ($((G''/G')_{LVD} > 1$) and, as the magnetic field increases, they progressively become more solid than liquid ($((G''/G')_{LVD} < 1$), due to the formation of increasingly stronger magnetic field-induced structures, in agreement with results of steady-state experiments. This magnetic field-induced fluid-solid transition is illustrated in Fig. 12.

Frequency sweeps In the absence of applied magnetic field, the frequency dependence in LVD shows similar trends for both systems with the loss modulus dominating over the storage modulus for most of studied frequency range (Fig. 13). The main qualitative difference is the higher values of both G′ and G″ for NPs-DOPA/sodium alginate system than for NPs-APTES/sodium alginate system, which could be explained on the same basis as the higher viscosity values for the former than for the latter discussed above for magnetoviscous effect. Moreover, a tendency of G′ to level at low frequency is experimentally observed. This tendency is typical of gel-like systems, although in these cases, G′ is higher than G″. Nevertheless, we could interpret this behavior as an indication of the existence of some bulk-like structure in the nanoparticle/sodium alginate systems. Note that this hypothesis was also required to explain the existence of non-negligible value of shear stress at 0.1 s^{-1} in the absence of applied magnetic field (see "Steady state").

As observed in Fig. 14, the most evident effect of applied magnetic field on the frequency dependence of G′ and G″ for the two nanoparticle/sodium alginate systems is an enhancement of the values of both G′ and G″ as the strength of magnetic field is increased from zero field. As above for the magnetoviscous effect and for results of amplitude sweeps, this is an indication of the strengthening of the microstructure of the systems by the effect of the applied magnetic field. In addition, note that G′ tends to increase along the whole range of frequency as the magnetic field reaches its highest values, especially for NPs-DOPA/sodium alginate system. In fact, trends for G′ and G″ for NPs-DOPA/sodium alginate system

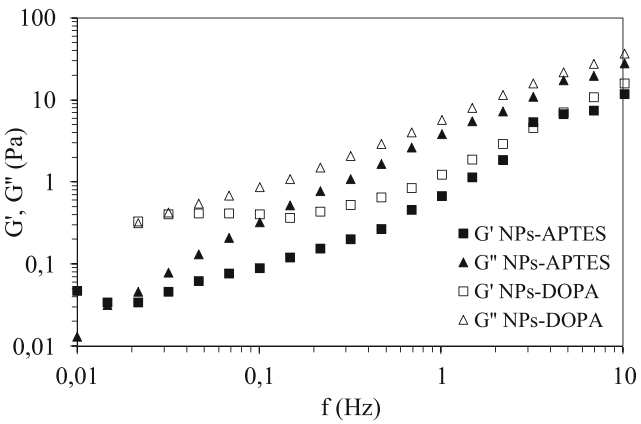

Fig. 13 Frequency dependence for NPs-APTES/sodium alginate mixtures and for NPs-DOPA/sodium alginate systems in the absence of applied magnetic field

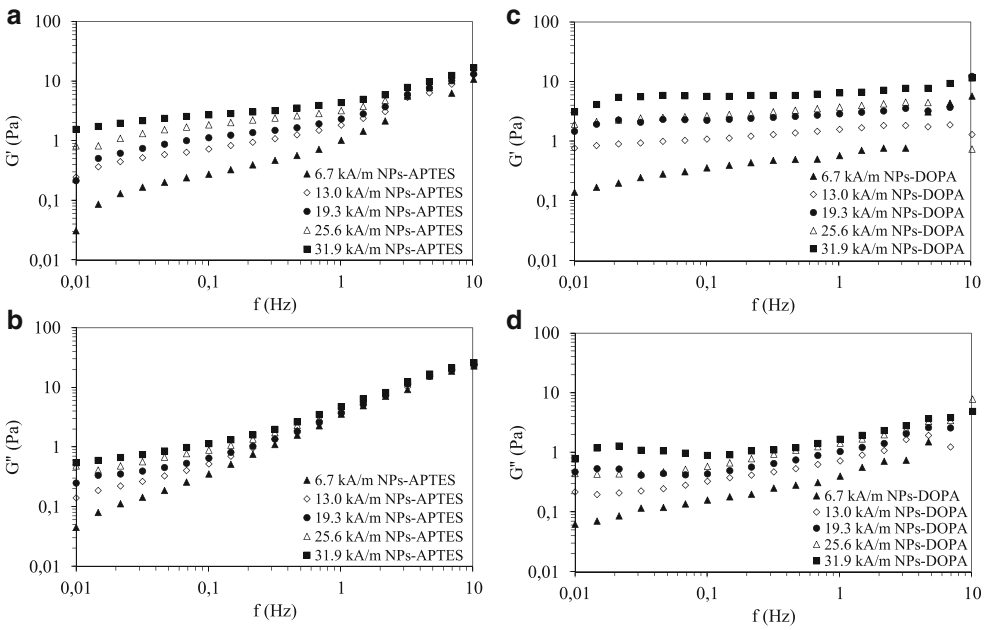

Fig. 14 Frequency dependence for NPs-APTES/sodium alginate (**a**, **b**) system and for NPs-DOPA/sodium alginate system (**c**, **d**) at different values of applied magnetic field

at the highest fields are similar to the ones of rubber (Macosko 1994), with G′ (larger than G″) being approximately constant, with a slight increase at the highest frequencies—and G″ showing a slight tendency to increase along the whole frequency range. Again, this seems to be an indication of the existence of a bulk-like microstructure in the case of NPs-DOPA/sodium alginate system, which is strengthened by the applied magnetic field.

Microscopic observations

In order to corroborate our previous hypothesis on the existence of some particle/polymer aggregates and/or internal percolating structures in nanoparticle/polymer system, we performed microscopic observations using laboratory made special device allowing the application of a magnetic field during the observations (Galindo-Gonzalez et al. 2014). As observed, in the absence of applied magnetic field, both NPs-APTES/sodium alginate system and NPs-DOPA/sodium alginate system show some large and dark aggregates (Fig. 15). Since the concentration of particles in sodium alginate aqueous solution is only 1 vol.%, these dark aggregates should be constituted by both particles and polymers, as depicted in Fig. 7. Interestingly, aggregates seem larger in the case of NPs-DOPA/sodium alginate system (in agreement with our previous hypothesis—see, for example, discussion related to Fig. 7). In addition, it seems that there are connections between

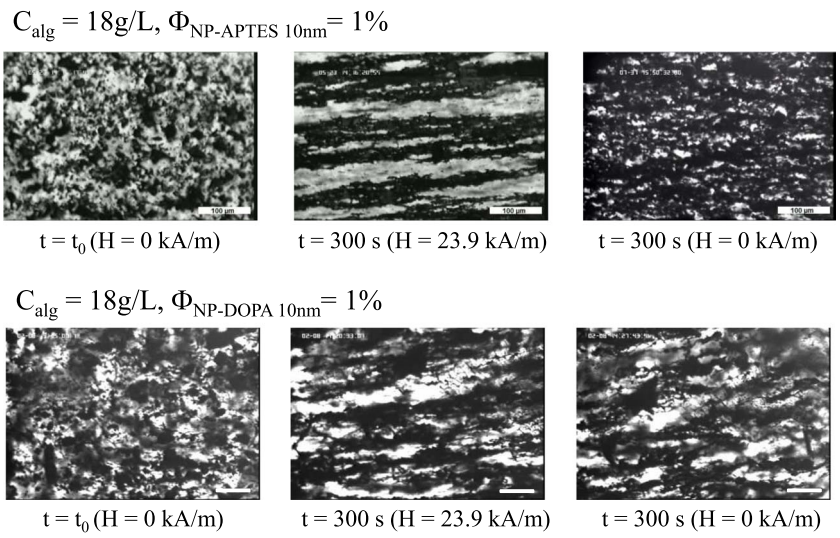

Fig. 15 Optical microscopy under magnetic field application for NPs-APTES/sodium alginate system and NPs-DOPA/sodium alginate system. Bar scale 100 μm

different aggregates in such a way that a three-dimensional network is present along the whole observation field. Concerning magnetic field application, as observed, its effect is slightly different for NPs-APTES/sodium alginate system than for NPs-DOPA/sodium alginate system (Fig. 15). For the former, some clear chain-like bands, separated by regions with negligible concentration of particles, are induced. On the other hand, for the latter, we observe only a tendency of the network to be deformed presenting a privileged direction along the magnetic field. Again, these observations are in agreement with our previous hypotheses: that NPs-APTES/sodium alginate system is composed of some short-range aggregates consisting of particles and polymers, whereas NPs-DOPA/sodium alginate system is mainly formed by a flocculated network consisting of particles and polymers linked by electrostatic forces. Finally, as observed in the last column of Fig. 15, once the magnetic field was switched off, the systems partially recovered the initial isotropic structure, although some privileged direction remained.

Conclusion

This study shows that the nature of ligand bonding on the surface of functionalized maghemite nanoparticles (NPs) synthesized by polyol process and introduced at low volume fraction in aqueous solutions of sodium alginate to elaborate composites can modulate the interactions between positively charged NPs and negatively charged biopolymer chains. The rheological properties of these smart composites are varied consequently. The changes of field-induced increase of low shear viscosity or magnetoviscous effect as well as the increase of elastic and viscous moduli in the linear viscoelastic domain have been explained by the formation of compact or loose aggregates between NPs and polymer chains. These findings have been experimentally confirmed by optical microscopic observation under applied magnetic field.

Funding information M.T. Lopez-Lopez received financial support by project FIS2017-85954-R (Ministerio de Economía, Industria y Competitividad, MINECO, and Agencia Estatal de Investigación, AEI, Spain, cofunded by Fondo Europeo de Desarrollo Regional, FEDER, European Union).

References

Basti H, Ben Tahar L, Smiri LS, Herbst F, Vaulay MJ, Chau F, Ammar S, Benderbous S (2010) Catechol derivatives-coated Fe3O4 and γ-Fe2O3 nanoparticles as potential MRI contrast agents. J Colloid Interface Sci 341:248–254. https://doi.org/10.1016/j.jcis.2009.09.043

Batchelor GK (1977) The effect of Brownian motion on the bulk stress in a suspension of spherical particles. J Fluid Mech 83:97–117. https://doi.org/10.1017/S0022112077001062

Bossis G, Lançon P, Meunier A et al (2013) Kinetics of internal structures growth in magnetic suspensions. Physica A A392:1567–1576. https://doi.org/10.1016/J.physa.2012.11.029

Brazel CS (2009) Magnetothermally-responsive nanomaterials: combining magnetic nanostructures and thermally-sensitive polymers for triggered drug release. Pharm Res 26:644–656. https://doi.org/10.1007/s11095-008-9773-2

Camargo PHC, Satyanarayana KG, Wypych F (2009) Nanocomposites: synthesis, structure, properties and new application opportunities. Mater Res 12:1–39. https://doi.org/10.1590/S1516-14392009000100002

Charron G, Hühn D, Perrier A, Cordier L, Pickett CJ, Nann T, Parak WJ (2012) On the use of pH titration to quantitatively characterize colloidal nanoparticles. Langmuir 28:15141–15149. https://doi.org/10.1021/la302570s

Creager SE, Clarke J (1994) Contact-angle titrations of mixed .omega.-mercaptoalkanoic acid/alkanethiol monolayers on gold. reactive vs nonreactive spreading, and chain length effects on surface pKa values. Langmuir 10:3675–3683. https://doi.org/10.1021/la00022a048

Doublier JL, Launay B (1981) Rheology of galactomannan solutions: comparative study of guar gum and locust bean gum. J Texture Stud 12:151–172. https://doi.org/10.1111/j.1745-4603.1981.tb01229.x

Fouineau J, Brymora K, Ourry L et al (2013) Synthesis, Mössbauer characterization, and Ab initio modeling of Iron oxide nanoparticles of medical interest functionalized by dopamine. J Phys Chem C 117:14295–14302. https://doi.org/10.1021/jp4027942

Galindo-Gonzalez C, Gantz S, Ourry L et al (2014) Elaboration and rheological investigation of magnetic sensitive nanocomposite biopolymer networks. Macromolecules 47:3136–3144. https://doi.org/10.1021/ma402655g

Galindo-Gonzalez C, Ponton A, Bee A, Chevalet J, Talbot D, Perzynski R, Dubois E (2016) Investigation of water-based and oil-based ferrofluids with a new magnetorheological cell: effect of the microstructure. Rheol Acta 55:67–81. https://doi.org/10.1007/s00397-015-0892-5

Hanini A, Schmitt A, Kacem K, Chau F, Ammar S, Gavard J (2011) Evaluation of iron oxide nanoparticle biocompatibility. Int J Nanomedicine 6:787–794. https://doi.org/10.2147/IJN.S17574

Haraguchi K, Murata K, Takehisa T (2012) Stimuli-responsive Nanocomposite gels and soft nanocomposites consisting of inorganic clays and copolymers with different chemical affinities. Macromolecules 45:385–391. https://doi.org/10.1021/ma202114z

Jeon I-Y, Baek J-B (2010) Nanocomposites derived from polymers and inorganic nanoparticles. Materials 3:3654–3674. https://doi.org/10.3390/ma3063654

Kane V, Mulvaney P (1998) Double-layer interactions between self-assembled monolayers of ω-mercaptoundecanoic acid on gold surfaces. Langmuir 14:3303–3311. https://doi.org/10.1021/la971296y

Laurent S, Forge D, Port M, Roch A, Robic C, Vander Elst L, Muller RN (2008) Magnetic Iron oxide nanoparticles: synthesis, stabilization, vectorization, physicochemical characterizations, and biological applications. Chem Rev 108:2064–2110. https://doi.org/10.1021/cr068445e

Liu F, Urban MW (2010) Recent advances and challenges in designing stimuli-responsive polymers. Prog Polym Sci 35:3–23. https://doi.org/10.1016/j.progpolymsci.2009.10.002

Lopez-Lopez MT, Kuzhir P, Zubarev A (2014) Effect of drop-like aggregates on the viscous stress in magnetic suspensions. J Non-Newtonian Fluid Mech 208–209:53–58. https://doi.org/10.1016/j.jnnfm.2014.04.001

Macosko CW (1994) Rheology: principles, measurements, and applications. p. 294, Wiley-VCH Publishers. Inc

Morales MA, Finotelli PV, Coaquira JAH et al (2008) In situ synthesis and magnetic studies of iron oxide nanoparticles in calcium-alginate

matrix for biomedical applications. Mater Sci Eng C 28:253–257. https://doi.org/10.1016/j.msec.2006.12.016

Nishio Y, Yamada A, Ezaki K et al (2004) Preparation and magnetometric characterization of iron oxide-containing alginate/poly(vinyl alcohol) networks. Polymer 45:7129–7136. https://doi.org/10.1016/j.polymer.2004.08.047

Odenbach S, Thurm S (2002) Magnetoviscous effects in ferrofluids. In: Odenbach S (ed) Ferrofluids: magnetically controllable fluids and their applications. Springer, Berlin, pp 185–201

Rayment P, Ross-Murphy SB, Ellis PR (1995) Rheological properties of guar galactomannan and rice starch mixtures— I. steady shear measurements. Carbohydr Polym 28:121–130. https://doi.org/10.1016/0144-8617(95)00110-7

Ren Y, Ellis PR, Sutherland IW, Ross-Murphy SB (2003) Dilute and semi-dilute solution properties of an exopolysaccharide from Escherichia coli strain S61. Carbohydr Polym 52:189–195. https://doi.org/10.1016/S0144-8617(02)00289-8

Richter A, Paschew G, Klatt S et al (2008) Review on hydrogel-based pH sensors and microsensors. Sensors 8:561–581. https://doi.org/10.3390/s8010561

Ridi F, Bonini M, Baglioni P (2014) Magneto-responsive nanocomposites: preparation and integration of magnetic nanoparticles into films, capsules, and gels. Adv Colloid Interf Sci 207:3–13. https://doi.org/10.1016/j.cis.2013.09.006

Rosensweig RE (1985) Ferrohydrodynamics. Cambridge University Press, Cambridge

Schexnailder P, Schmidt G (2009) Nanocomposite polymer hydrogels. Colloid Polym Sci 287:1–11. https://doi.org/10.1007/s00396-008-1949-0

Van Vlierberghe S, Dubruel P, Schacht E (2011) Biopolymer-based hydrogels as scaffolds for tissue engineering applications: a review. Biomacromolecules 12:1387–1408. https://doi.org/10.1021/bm200083n

Wang Q, Ellis PR, Ross-Murphy SB, Burchard W (1997) Solution characteristics of the xyloglucan extracted from Detarium senegalense Gmelin. Carbohydr Polym 33:115–124. https://doi.org/10.1016/S0144-8617(97)00026-X

Wang D, Nap RJ, Lagzi I, Kowalczyk B, Han S, Grzybowski BA, Szleifer I (2011) How and why nanoparticle's curvature regulates the apparent pKa of the coating ligands. J Am Chem Soc 133:2192–2197. https://doi.org/10.1021/ja108154a